# Hyperfine Structure and Zeeman Effect in Mercury Isotopes

Lulu Liu (Partner: Chris Chronopoulos)*
*MIT Undergraduate*
(Dated: April 24, 2008)

With the assistance of a Fabry-Perot interferometer, investigations in high resolution optical spectroscopy yield hyperfine components of the 5460.7 A line in even and odd isotopes of mercury. Analysis of the hyperfine data shows good agreement with the expected energy shift ratios of $^{199}$Hg and isotope broadening due to nuclear mass disparity, which we find to be $\Delta\lambda = (2.7 \pm .7) \times 10^{-3} A$. We arrive at a value for the hyperfine coupling constant, $a$, of $36.5 \pm 6.5$ hc/m. Data on the shift and splitting of the 5770 A, 5791 A, and 5461 A emission lines under the influence of a magnetic field allows us to calculate a value for the electron charge-to-mass ratio, e/m. Obtained in this way, e/m = $(1.86 \pm 0.30) \times 10^{11}$ A·s/kg.

## 1. INTRODUCTION

Here, we study the emission spectrum of mercury with two valence electrons. In the ground state these two electrons occupy the 6s ($n = 6$, $l = 0$) orbital with all lower energy levels completely filled. The effect of this arrangement is an fortunate simplication of the complex energetics of the problem. If we look only at transitions involving the two valence electrons, and view the system as a hydrogenic atom with two electrons, we can avoid individual treatment of the many-body problem, a task that is involved if not impossible. Two such transitions are the green 5461 A line emitted by the $7^3S_1$ to $6^3P_2$ transition, and the 5770 A and 5791 A yellow doublet resulting from transitions to the $6^1P_1$ orbital from their symmetric or antisymmetric spin state in the $6^3D_2$ and $6^1D_2$ orbitals. Here, spectroscopic notation has used the convention $n^{2S+1}L_J$ to denote initial and final states. We've introduced quantum numbers $S$ and $J$ to represent the vector sums of the spins and total angular momenta of the two valence electrons, respectively.

$$\vec{S} = \vec{s}_1 + \vec{s}_2 \tag{1}$$

$$\vec{J} = \vec{j}_1 + \vec{j}_2 \tag{2}$$

Eigenstates of the Hamiltonian with a spherically-symmetric coulombic potential are many-fold degenerate as their energies depend only on the principle quantum number, $n$. Small perturbations to the hamiltonian can be introduced by way of internal spin-spin coupling between the nucleus of a mercury atom and its valence electrons (known as hyperfine structure) or by the application of an external magnetic field (Zeeman effect). These energy perturbations serve to lift the degeneracy of states. Its effects, in terms of energy shift of atomic transitions, can be observed using the high resolution spectroscopic equipment available for this lab.

*Electronic address: lululiu@mit.edu

## 2. HYPERFINE THEORY

A necessary condition for hyperfine splitting of the valence energy levels in mercury is a nucleus with a non-zero spin. The perturbing Hamiltonian in this case is proportional to the coupling between the total nuclear spin, $I$, and total electron angular momentum, $J$,

$$H'_{hf} \propto I \cdot J \tag{3}$$

We introduce the quantity $F = I + J$ as a new quantum number to describe the states of the system, and use the relation,

$$F^2 = (I + J)^2 = I^2 + J^2 + 2I \cdot J \tag{4}$$

to replace $I \cdot J$ in the Hamiltonian. First order perturbation theory then yields the correction to the energy levels of the mercury atom.

$$\Delta E_{hf} = \frac{a}{2}[F(F+1) - J(J+1) - I(I+1)] \tag{5}$$

where $a$ is introduced as the hyperfine coupling constant. When applied to the mercury atom, we expect all even isotopes, isotopes with an even number of protons and total nucleons, with $I = 0$, to exhibit no hyperfine splitting of the energy levels. We later verify this prediction in the green 5461 A line.

## 3. ZEEMAN EFFECT

As mentioned earlier, application of an external magnetic field lifts the degeneracy in states with different angular momenta along the axis of the magnetic field. Along much of the same lines as hyperfine structure, this shift in energy is also the result of interaction between a magnetic dipole created by a spinning charge and an established magnetic field. The perturbing Hamiltonian in this case, and the resulting shifts in energy, are

$$H'_Z = -\vec{\mu} \cdot \vec{B} \tag{6}$$

$$\Delta E_Z = -(g\mu_B B_z) m_J \tag{7}$$

$\mu_B$ is the bohr magneton, $\mu_B = \frac{\hbar}{2}\left(\frac{e}{m}\right)$ in SI units, $B_z$ is the strength of the external magnetic field, and $m_J$ is the total spin of the electrons along the z-direction. $g$ is a ratio known as the landé g-factor, and weights the orbital and spin angular momenta according to the gyromagnetic ratio of the electron. Again derived using perturbation theory[1], the g-factor can be calculated with,

$$g = 1 + \frac{J(J+1) - L(L+1) + S(S+1)}{2J(J+1)} \tag{8}$$

Measurement of the energy shift using interferometry yields $\Delta E$, and with knowledge of the initial and final spin states of the transition and the external magnetic field strength, a simple calculation yields a value for the Bohr magneton and consequently a much revered quantity in physics, the electron charge-to-mass ratio, $\frac{e}{m}$.

Additionally, we hope to verify that the spin of the photon emitted during these transitions is consistent with angular momentum conservation. By application of a magnetic field, we've selected a preferred direction out of all possible directions for polarization of the emitted light. Radiation emitted from transitions with $\Delta m = \pm 1$ are circularly polarized around the z-axis, and those with $\Delta m = 0$ are circularly polarized around some perpendicular axis. We are observing from a direction perpendicular to the axis of the applied magnetic field. Consequently, we expect to see $\pi$ and $\sigma$ linearly polarized light from the $\Delta m = 0$ and $\Delta m = \pm 1$ transitions, respectively.

## 4. EQUIPMENT

The Fabry-Perot interferometer selects for constructive interference between multiply reflected and parallel rays of light emerging from the far side of a pair of closely-spaced partially silvered mirrors. When focused by a lens, the interference maxima form concentric circles with higher order reflections toward the center. The condition for interference maxima is as follows,

$$2Dcos\theta = m\lambda \tag{9}$$

where $D$ is the plate separation (which we take to be always approximately 2.8mm), $\theta$ is the angle of incidence of light, $\lambda$ is the wavelength, and $m$ is the order of interference. Piezoelectric crystals have been installed between the mirrors, voltage applied to the crystals cause them to expand and contract, such that the separation $D$ is linearly related to the applied voltage $V$. In order to retrieve useful spectroscopic data on the corresponding wavelength differences associated with pairs of interference maxima of the same order viewable on the scope, we use the following equation derived in the 8.14 Lab Guide [2],

$$\delta\lambda = \frac{\lambda^2}{2D}\frac{\delta D}{\Delta D} = \frac{\lambda^2}{2D}\frac{\delta V}{\Delta V} \tag{10}$$

Here, $\delta V$ is the voltage separation between the relevant maxima, and $\Delta V$ is the separation between different orders of interference. In varying the voltage periodically, we can scan the interference spectrum obtained by observing the intensity at a single point on the focal plane. We choose this point to be the center of the concentric circles due to maximum integrated signal. We collect intensity spectra as a function of time using a photomultiplier, the data appears on two channels of the oscilloscope.

## 5. DATA

An example of the raw data obtained in this experiment is shown in Figure 1. Note the voltage ramp's deviation from linear behavior. This is indicative that a simple scaling of the x-axis of the peak profile will result in a systematic "spreading" of the peaks toward higher voltages. In order to eliminate this potential error, we take advantage of the parametrization of both quantities (intensity and voltage) by the time bins along the x-axis of the oscilloscope and obtain a curve of measured intensity against measured voltage.

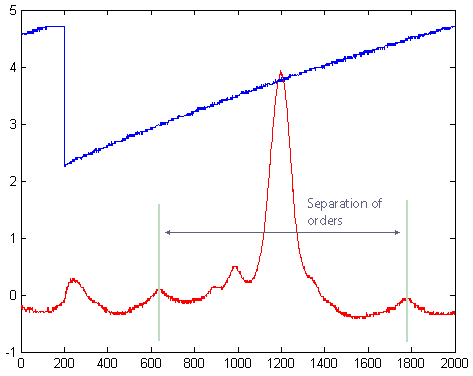


FIG. 1: The figure shows the two channels, 1 (blue) and 2 (red), recorded on the oscilloscope. Channel 1 measures the applied voltage, while Channel 2 measures the recorded intensity at a fixed location on the focal plane. Periodicity is a measure of $\Delta V$.

## 6. HYPERFINE STRUCTURE OF THE GREEN LINE

Figure 2 is the calibrated curve showing some hyperfine features of the 5461 A green mercury line. The even isotopes of mercury all exhibit a single (broadened) peak, while $^{199}$Hg with nuclear spin $I = 1/2$ and $^{201}$Hg with $I = 3/2$ both exhibit hyperfine structure to varying degrees. The transitions responsible for each identifiable peak is given in Table I. According to Steinfeld [3], hyperfine structure in $^{199}$Hg splits the green line into three peaks with energies with distinct energies while in $^{201}$Hg, eight distinct peaks should be present. While we are only

able to resolve three out of the eight $^{201}$Hg lines, we see the entire hyperfine structure of $^{199}$Hg. Thus, the remainder of the analysis will deal with this latter isotope.

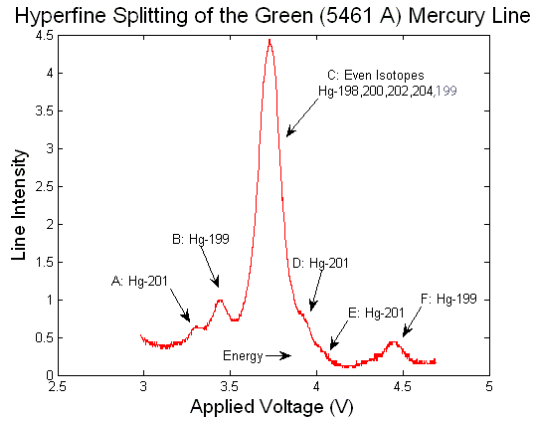


FIG. 2: Hyperfine splitting of various isotopes. Peaks identified with the help of Steinfeld's discussion on atomic physics [3].

| Peak | Isotope | Nuclear Spin I | Initial F = J + I | Final F |
|---|---|---|---|---|
| A | Hg-201 | 3/2 | 1/2 | 1/2 |
| B | Hg-199 | 1/2 | 1/2 | 3/2 |
| C | Hg-199 | 1/2 | 3/2 | 5/2 |
| | Hg-198,200,202,204 | 0 | 1 | 2 |
| D | Hg-201 | 3/2 | 5/2 | 7/2 |
| E | Hg-201 | 3/2 | 5/2 | 1/2 |
| F | Hg-199 | 1/2 | 3/2 | 3/2 |

TABLE I: Corresponding transitions for labeled peaks in Figure 2.

Peaks B, C, and F correspond to transitions within the $^{199}$Hg atom. Using the hyperfine theory in section 2, we derive a ratio for the expected peak separations.

$$R = \Delta E_{BC} : \Delta E_{CF} : \Delta E_{BF} = 1 : 2.5 : 3.5 \tag{11}$$

From our data we extract an experimental verification of the hyperfine prediction. We obtain a ratio of $R = 1 : (2.4 \pm 0.1) : (3.5 \pm 0.1)$. In addition, we obtain a value for the hyperfine coupling constant, $a$, by considering the energy difference between the transitions presented by peaks B and C. This value we find to be $a = 36.5 \pm 7.1$ hc/m.

Even isotopes of mercury, though unsplit by the hyperfine interaction, are not expected to be degenerate, either. A phenomenon known as isotope shift is used to describe the effect of a finite mass nucleus. The result is a slight adjustment in the mass of the electron: here we use a reduced mass $\mu = m_e \frac{M}{M+m_e}$ orbiting around the center of mass of the system and all other physics remains unchanged. The correction in energy is small but measurable:

$$E' = E_0 \left(1 - \frac{m_e}{N m_p}\right) \tag{12}$$

where $E_0$ is the energy assuming infinite nuclear mass, and $N$ is the number of nucleons. A difference in $N$ between $^{204}$Hg, the heaviest isotope, and $^{198}$Hg, the lightest, leads to a spread in energy,

$$\frac{\Delta E_{is}}{E_0} = \frac{\left(1 - \frac{m_e}{204 m_p}\right)}{\left(1 - \frac{m_e}{198 m_p}\right)} - 1 = 5 \times 10^{-7} \tag{13}$$

The corresponding predicted spread in wavelength is $\lambda \approx 0.003A$. A sharp hyperfine peak in the $^{199}$Hg spectrum serves as a baseline measure of resolution limit. Fitting peak F to a gaussian, we find a width of $\sigma_F = 0.0180 \pm 0.0007A$. A gaussian fit of peak C containing all even isotopes yields a width of $\sigma_C = 0.0207 \pm 0.0001A$. The result is an isotope spread $\Delta\lambda = (2.7 \pm .7) \times 10^{-3}$ A. The predicted value falls nicely within our error bars. We've now confirmed hyperfine structure and isotope shift in the green 5461 A line of mercury.

## 7. MAGNETIC FIELD CALIBRATION

Precise measurement of the applied external magnetic field is crucial to the next portion of our experiment. A dual-core electromagnet generates a magnetic field that increases in intensity with the current flowing through it. Using a Hall probe, we measure the B-field between the magnets at the location of the mercury lamp repeatedly for several different applied currents. The results are plotted in Figure 3, and used to extrapolate a reliable value of magnetic field strength based on measured current.

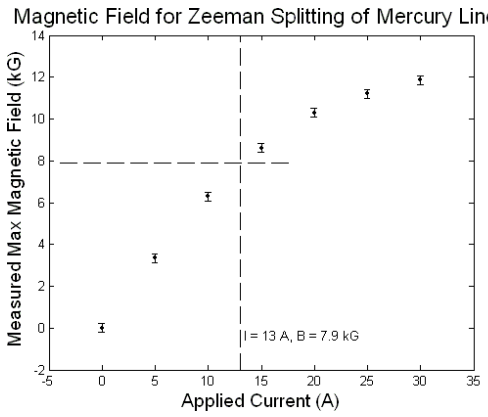


FIG. 3: Calibration curve for electromagnets.

## 8. ZEEMAN SPLITTING OF MERCURY LINES

The Zeeman split energy level diagram and transitions for states involved in emission of the green line of mercury is shown in Figure 4. Likewise, a diagram of the transitions involved in the yellow doublet is given in Figure 5. We attempt to verify this structure using the optical spectroscopy methods developed thusfar.

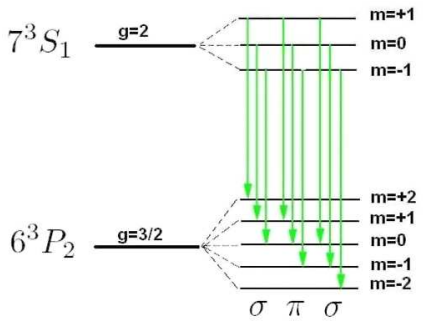


FIG. 4: The Zeeman effect splits the green mercury line into 9 transitions between states with different angular momenta in the z-direction. The difference in g-factor ensures each transition has a distinct energy.

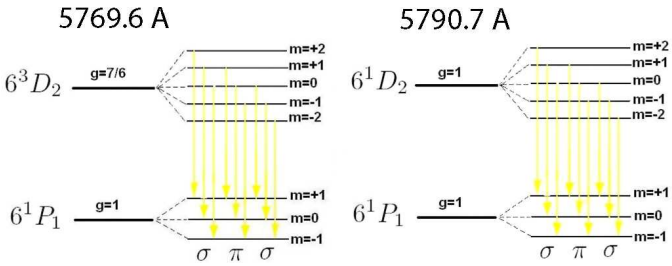


FIG. 5: Similarly, each yellow line is also split into 9 components, however, due to g-factors that are either identical or close to identical between the upper and lower levels, we only observe each line split into three resolvable energy peaks.

Photographs of the interference pattern alongside the spectroscopic data obtained with and without linear polarizers can be seen in Figures 6 and 7 for both the green line and the yellow doublet of mercury. We see that our observations corroborate our theoretical predictions given both in this section and section 3. In particular, we observe a split into nine lines from one in the green transition, and a split into a total of six lines from two in the yellow transitions. Furthermore, the radiation is polarized in the predicted manner.

From these results we are now at the liberty of calculating the electron charge-to-mass ratio. With knowledge of the initial and final states that produce each split line, by selecting pairs of lines with the initial $m_J$ state in common and a final $m_J$ state differing by $\pm 1$, we can convert the measured difference in energy between these two transitions immediately into the quantity $g\mu_B B$ representing the spacing between each adjacent energy level split by the Zeeman interaction.

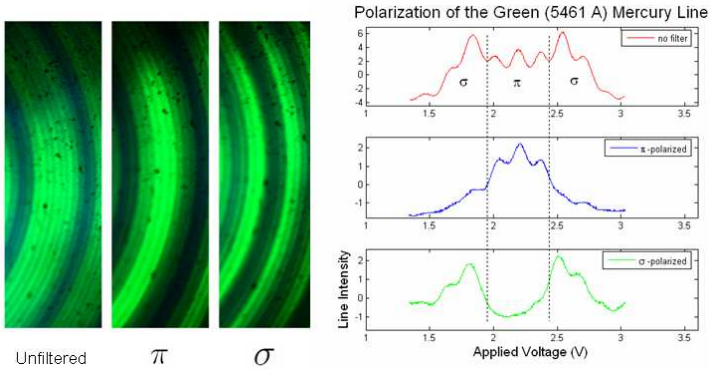


FIG. 6: Zeeman splitting of the 5460.7 A line of mercury under a 7.9 kG applied field.

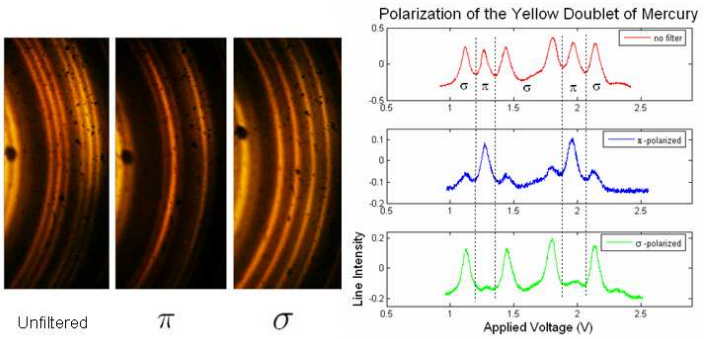


FIG. 7: Zeeman splitting of the 5460.7 A line of mercury under a 3.6 kG applied field.

$$\frac{e}{m} = \frac{2\pi c}{DBg}\left(\frac{\delta V}{\Delta V}\right) \tag{14}$$

The errors propagated from each of the measured quantities follows:

| Quantity | Value | Error |
|---|---|---|
| D | 2.8 mm | ± 0.3 mm |
| B | 7.9 kG | ± 0.4 kG |
| $\delta$ V | varies | ± 30 mV |
| $\Delta$ V | 1.5 V | ± 30 mV |
| g | 3/2 | – |

We obtain for the charge-to-mass ratio, taking an average of the $\frac{e}{m}$ values obtained through selection of different pairs of lines (see Table II):

$$\mu_B = (9.61 \pm 1.58) \times 10^{-24} J/T \tag{15}$$

$$\frac{e}{m} = (1.86 \pm 0.30) \times 10^{11} \text{A*s/kg} \tag{16}$$

| Line Pair | e/m ($10^{11}$ A*s/kg) |
|---|---|
| 3 and 6 | 1.89 ± 0.56 |
| 2 and 5 | 1.89 ± 0.56 |
| 5 and 8 | 1.78 ± 0.51 |
| 4 and 7 | 1.90 ± 0.56 |

TABLE II:

## 9. ELABORATION ON ERRORS

The baseline uncertainty (∼15%) on plate separation, $D$, dominated the random error on most of our calculated quantities. This is mostly due to the difficulty of determining plate separation from three uncertain and usually all very different readings from three coarse adjustment knobs. Of course, since over the course of an experimental period, we did not often readjust the coarse plate separation, here, we have also a source of possible systematic error. If the distance, $D$, that found its way into many of our key equations turned out to be an over- or under- estimate of the actual distance, our entire analysis would be systematically skewed.

Our resolution limit depended heavily on our ability to focus the instrument chain. A poor focus often resulted in unresolvable peaks. Patience and luck were both necessary in order to limit this major source of uncertainty. However, human error and instrumental limit are not the sole causes for peak broadening. Doppler broadening, usually a neglectible quantity in spectroscopic experiments, is on the order of $\Delta\lambda = 0.003A$, which is actually resolvable with the precision of our instruments (recall the isotope broadening results).

The non-linearity of the voltage bias ramp, though a possible cause of additional systematic error, was, we believe, adequately treated and eliminated through the deparametrization exercise. The magnitude of the magnetic field varied somewhat with time and could only be measured roughly by various orientations of the Hall probe is another uncertain quantity which we were unable to make more precise. The error on this particular quantity was assessed with repeated trials.

## 10. CONCLUSIONS

We've accomplished the main objectives of this experiment. We verified the validity of the quantum mechanical models (including the vector model) used to analyze the two valence electron system of the mercury atom, and the high resolution capability of the Fabry-Perot interferometer. We assessed various energetic interactions that break the degeneracies present in the coulombic treatment of the atom. These include the hyperfine structure of the atom, the isotope shift due to finite nuclear mass, and the Zeeman external field effect. Along the way, we confirmed angular momentum conservation in the process of atomic photon emission by confirming linear polarization along two perpendicular directions for both the green and the yellow lines of mercury.

From these results we derived several important quantities. Most important is the charge-to-mass ratio of the electron, which we found to be an astoundingly huge $(1.86 \pm 0.30) \times 10^{11}$A*s/kg, and contained within its errorbars the accepted value of $1.76 \times 10^{11}$A*s/kg . Also, we obtained a value for the hyperfine coupling constant, $a$, which, to reiterate, was 36.5 ± 7.1 hc/m. The very small isotope shift was somehow measureable using the equipment at our disposal, which we found to be $\Delta\lambda = (2.7 \pm .7) \times 10^{-3}A$, which also agreed within uncertainty with the expected spread of 0.003 A. The consistent agreement of our results with quantum mechanical predictions verified the validity of our many assumptions, and reaffirmed us in our ability to simplify and thus investigate very complex systems.


[1] A. Melissinos, *Experiments in Modern Physics.* [1966]
[2] Sewell, "Mossbauer Spectroscopy", 8.14 Course Reader, [2007]
[3] J. Steinfeld, *Molecules and Radiation.* MIT Press. [2003]
[4] A. Melissinos, *Experiments in Modern Physics, 2nd Edition.* Academic Press. [2003]



### Acknowledgments

All non-linear fits were made with the MATLAB scripts made available to us on the Junior Lab website: http://web.mit.edu/8.13/www/jlmatlab.shtml.

We would like to thank the Junior Lab staff for their assistance.